Anticrossing spectroscopy of K Rydberg atoms using 300-K blackbody radiation

R. C. Stoneman, G. Janik, and T. F. Gallagher
Department of Physics, University of Virginia, Charlottesville, Virginia 22901
(Received 31 March 1986)

The avoided crossings in an electric field of K s and p states with the nearly hydrogenic Stark manifold states have been investigated using 300-K blackbody radiation. Anticrossings between states of the same $|m_j|$ for which the $|m_l|$ values are the same or differ by one are encountered. The anticrossings between states of the same $|m_l|$ are quite wide as they are due to core penetration and polarization effects. The anticrossings for which $|m_l|$ differs by one are produced by the spin-orbit interaction and are accordingly quite small. We present results for the ns states for n in the range 18—29 and for the np states for n in the range 19—23.

I. INTRODUCTION

Level crossing[1] and anticrossing[2] spectroscopy, techniques based on the crossing or near crossing of atomic energy levels in an external field, have been widely used in the past to measure properties of atomic excited states. Specifically these techniques have yielded measurements of fine and hyperfine structure, Stark and Zeeman shifts, oscillator strengths, and lifetimes.[3–5] In addition to being a useful artifact, the avoided crossings in an electric field have recently been recognized as intrinsically important factors in static[6] and dynamic[7] field ionization of Rydberg atoms.

The electric-field-induced avoided crossings of Rydberg-atom energy levels have previously been directly measured by laser spectroscopy.[8] However, this technique is limited to levels which do not approach each other more closely than the laser linewidth. For typical pulsed lasers this limit is about 5 GHz. For avoided crossings narrower than this, rf spectroscopy has been used to accurately measure the separation at the avoided crossing.[6] The rf technique, however, has the limitation that one of the levels must be preferentially excited and one preferentially detected. These conditions are not met for all avoided crossings. Also, the rf technique is inherently two dimensional, requiring rf scans to be taken at several electric field values in order to find the point of closest approach.

We elaborate here on our earlier report[9] of a new method of anticrossing spectroscopy using 300-K blackbody radiation. The technique is straightforward and yields good results even for those situations where the rf technique is least sensitive. In this report we develop the theory of the anticrossing signals that we observe, and present new data with improved resolution. We also describe our investigations of other techniques for observing anticrossing signals which are, in principle, attractive. As we shall see these alternatives are not as useful as the blackbody-radiation method.

II. THEORY

As two Stark-shifted atomic levels approach each other with a change in the electric field, any perturbation which couples the levels will cause them to repel. In hydrogen there is no perturbation save the negligibly small spin-orbit interaction and the levels cross, for all practical purposes. In the alkali metals the interaction of the valence electron with the ion core introduces a perturbation between atomic levels with the same value of $|m_l|$. The dotted lines of Fig. 1 show two levels $|a\rangle$ and $|b\rangle$ which cross when the perturbation between them is ignored. When the perturbation V is included we obtain the real eigenstates $|u\rangle$ and $|l\rangle$ (solid curves in Fig. 1). The eigenstates are superpositions of the unperturbed states and consist of 50-50 mixtures at the point of closest approach. At a specific electric field the energies of states $|a\rangle$ and $|b\rangle$ are given by the complex energies W_a and W_b which are given by

$$W_a = E_a - i\Gamma/2 , \tag{1}$$

$$W_b = E_b - i\Gamma/2 , \tag{2}$$

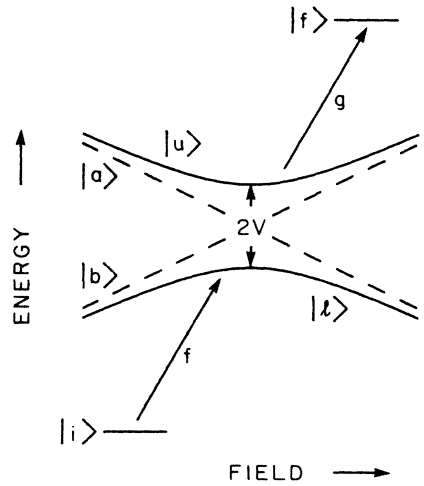

FIG. 1. Stark states $|a\rangle$ and $|b\rangle$ cross when the perturbation between them is ignored. The real states $|u\rangle$ and $|l\rangle$ result from the perturbation V. In our experiment the initial state $|i\rangle$ is the $4p$ state of potassium. The laser excitation is represented by f, and the blackbody excitation by g.

The imaginary parts of W_a and W_b allow for the radiative decay of these levels at a rate Γ. For simplicity we have assumed Γ to be the same for $|a\rangle$ and $|b\rangle$. If the off-diagonal matrix element coupling $|a\rangle$ and $|b\rangle$ is given by V the superposition can be parameterized in the following way:

$$|u\rangle=(\cos\theta)|a\rangle+(\sin\theta)|b\rangle , \tag{3}$$

$$|l\rangle=(-\sin\theta)|a\rangle+(\cos\theta)|b\rangle , \tag{4}$$

where

$$\tan(2\theta)=\frac{2V}{E_a-E_b},\quad 0\le\theta\le\pi/2 . \tag{5}$$

In our experiment we excite the eigenstates with a pulsed dye laser. The laser linewidth is about 0.5 cm^{-1}, which is much larger than the closest approach of the eigenstates we have investigated (<1 GHz). This means that we excite both eigenstates when the field is near the avoided crossing. The pulse width of the laser is about 5 ns which implies a coherent bandwidth of roughly 100 MHz. If the states are separated by more than this amount we excite an incoherent mixture; if the spacing is less, we excite a coherent superposition. We shall show that with our technique, the same type of signal is obtained in either case so we shall consider explicitly the case of incoherent excitation. The radiative decay times, $1/\Gamma$, of these eigenstates are generally greater than 5 μs. Part, $\sim 10\%$, of this observed decay rate is due to excitation by the ambient 300-K blackbody radiation to higher excited states.[10] The anticrossing signals that we observe are a result of the interaction between the blackbody radiation and the eigenstates $|u\rangle$ and $|l\rangle$ near the avoided crossing.

As a model for our anticrossing signal we assume the following sequence of events. First a coherent or incoherent mixture of eigenstates is produced at a fixed dc electric field. This excitation is assumed to occur instantaneously at time $t=0$. Then the mixture of states evolves in time under the influence of the static atomic Hamiltonian and dc field. During this time these states are driven by blackbody radiation to a higher-lying atomic state which is assumed not to decay. Finally, at time $t=T$ the atoms in the higher excited state are selectively field ionized and detected.

To calculate the probability of an atom reaching the final state $|f\rangle$ we first calculate the probabilities P_u and P_l of reaching states $|u\rangle$ and $|l\rangle$. If f_a and f_b are the dipole matrix elements for excitation by the laser field E_L from the initial state $|i\rangle$ to states $|a\rangle$ and $|b\rangle$, i.e., $f_a=\langle a|\mu E_L|i\rangle$ and $f_b=\langle b|\mu E_L|i\rangle$ then P_u and P_l are given by

$$\begin{aligned} P_u&=|\langle u|\mu E_L|i\rangle|^2=(f_a\cos\theta+f_b\sin\theta)^2 ,\\ P_l&=|\langle l|\mu E_L|i\rangle|^2=(f_b\cos\theta-f_a\sin\theta)^2 . \end{aligned} \tag{6}$$

If we take the ratio f of these matrix elements, $f=f_b/f_a$, then Eq. (6) may be written

$$\begin{aligned} P_u&=(\cos\theta+f\sin\theta)^2/(1+f^2) ,\\ P_l&=(f\cos\theta-\sin\theta)^2/(1+f^2) . \end{aligned} \tag{7}$$

We note that $P_u+P_l=1$, independent of θ. In other words the total number of atoms excited to the pair of states u and l by the laser is independent of the field.

The probability of atom's having been driven to the final state $|f\rangle$ by a time T is given by

$$P(T)=\int_0^T (P_u g_u^2+P_l g_l^2)e^{-\Gamma t}dt , \tag{8}$$

where $g_u=\langle f|\mu E_B|u\rangle$ and $g_l=\langle f|\mu E_B|l\rangle$ are the blackbody-radiation matrix elements connecting the $|u\rangle$ and $|l\rangle$ states to the $|f\rangle$ state. Expressing g_u and g_l in terms of the analogous matrix elements from the $|a\rangle$ and $|b\rangle$ states which are $g_a=\langle f|\mu E_B|a\rangle$ and $g_b=\langle f|\mu E_B|b\rangle$ leads to

$$\begin{aligned} g_u^2&=(g_a\cos\theta+g_a\sin\theta)^2 ,\\ g_l^2&=(g_b\cos\theta-g_a\sin\theta)^2 . \end{aligned} \tag{9}$$

Introducing the ratio of the matrix elements $g=g_b/g_a$ leads to

$$\begin{aligned} g_u^2&=(\cos\theta+g\sin\theta)/(1+g^2) ,\\ g_l^2&=(g\cos\theta-\sin\theta)/(1+g^2) . \end{aligned} \tag{10}$$

Substituting into Eq. (8) the expressions of Eqs. (10) and (7) yields:

$$\begin{aligned} P(T)=&\left[\frac{(\cos\theta+f\sin\theta)^2(\cos\theta+g\sin\theta)^2}{(1+f^2)(1+g^2)}\right.\\ &\left.+\frac{(f\cos\theta-\sin\theta)(g\cos\theta-\sin\theta)}{(1+f^2)(1+g^2)}\right]\\ &\times\frac{1-e^{-\Gamma T}}{\Gamma} . \end{aligned} \tag{11}$$

If we now replace $\cos\theta$ and $\sin\theta$ using Eq. (5) we can rewrite Eq. (11) as

$$\begin{aligned} P(T)=&\left[(1+f^2g^2)+\left[\frac{(2V)^2}{(2V)^2+(E_a-E_b)^2}\right]\left[2fg-\frac{(f^2-1)(g^2-1)}{2}\right]\right.\\ &\left.+\left[\frac{(2V)(E_a-E_b)}{(2V)^2+(E_a-E_b)^2}\right][-f(g^2-1)-g(f^2-1)]\right]\left[\frac{1-e^{-\Gamma T}}{\Gamma}\right] . \end{aligned} \tag{12}$$

All the line-shape dependence is contained in the large square brackets of Eq. (12). To a good approximation f and g are constant and the unperturbed energies E_a and E_b have linear Stark shifts in the small region near an avoided crossing. In this approximation the first term in the brackets of Eq. (12) is a constant, the second a Lorentzian, and the third a dispersion curve. The Lorentzian and dispersion curves have equal centers and widths.

Although the anticrossing signal depends in a complicated way on both f and g several cases are fairly simple. If $f=g=1$ the signal is a pure Lorentzian with amplitude equal to the dc component. If $f=g=0$ the signal is a pure Lorentzian with amplitude $-\frac{1}{2}$ times the dc component. For some of the avoided crossings we investigated (the s-level anticrossings) the f and g values were determined to be ~ 3 by laser measurements away from the avoided crossings. This results in signals which have both Lorentzian and dispersion components.

Let us return for a moment to our earlier assertion that in our experiments, even if the separation of the $|u\rangle$ and $|l\rangle$ states is small enough that these states may be excited coherently, we would be unlikely to observe the coherence. It should be manifested as beats at the angular frequency ω_{u-l} corresponding to the $u-l$ energy spacing. First, as shown by Eq. (8) our signal is an integral, so that even if there was a modulation of depth δ in P_u and P_l the depth of modulation would be reduced to $\delta\Gamma/\omega_{u-l}$ in the physically meaningful case $\Gamma \ll \omega_{u-l}$. For a 50-MHz-wide avoided crossing and $1/\Gamma=5$ μs the ratio Γ/ω_{u-l} is 0.67×10^{-3}. It is unlikely that we would be able to detect a quantum beat modulation, usually not large to begin with,[11] after such a reduction. Second, our field ionization detector has a rise time of ~ 0.5 μs limiting observable beat frequencies to <1 MHz, which is below the detectable limit for our field inhomogeneity. Finally, we saw no dependence of the observed signals on delay time before applying the ionizing pulse. Thus we are confident that our earlier restriction to the case of incoherent excitation of the $|u\rangle$ and $|l\rangle$ states is adequate for the description of our problem.

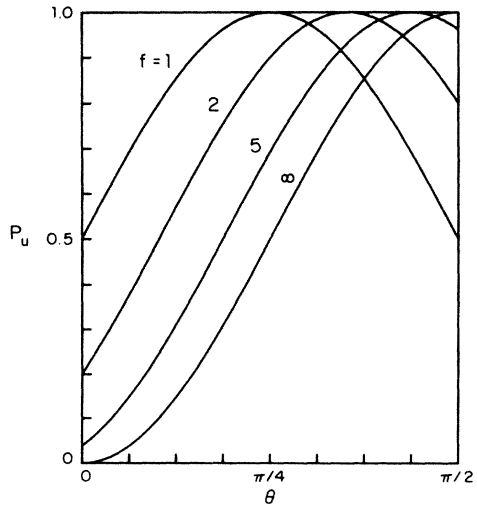

FIG. 2. Normalized probability for excitation to the real upper state $|u\rangle$, as a function of the crossing parameter θ. P_u is shown for several positive values of $f=f_b/f_a$. For negative f, $P_u(\theta,-f)=1-P_u(\pi/2-\theta,f)$. For the lower state $|l\rangle$, $P_l=1-P_u$.

At this point it is interesting to digress for a moment to consider the alternative approach of using rf spectroscopy in conjunction with the same broadband exciting laser. The excitation probability P_u is plotted in Fig. 2 for several values of f. For $f=1$ the two eigenstates have equal excitation probability away from the avoided crossing. At the point of closest approach, $\theta=\pi/4$, the excitation is all directed into the $|u\rangle$ state. If an rf field is applied with frequency $\nu=2$ V/h the level populations will equalize and a sharp increase (decrease) of the field ionization of the $|l\rangle$ ($|u\rangle$) state will occur. This situation is most favorable for the rf measurement technique. As f increases, the relative excitation probability P_u/P_l at the point of closest approach decreases until at very large f values $P_u=P_l$. The rf technique is therefore very insensitive for large values of f.

III. EXPERIMENTAL PROCEDURE

Observation of the anticrossing signals described here requires an experimental arrangement very similar to that used in previous field ionization studies.[12] A beam of potassium atoms passes between two electric field plates 1.590(1) cm apart. The atoms are stepwise excited by two pulsed dye lasers, from the $4s$ the $4p_{1/2}$ or $4p_{3/2}$ state with the "red" laser, and then from the $4p$ to the desired Rydberg state with the "blue" laser. The lasers are linearly polarized either parallel or perpendicular to the electric field, depending on the state desired. A dc voltage is applied to the plates, exposing the atoms to a uniform electric field. Approximately 3 μs after the laser pulses, a high-voltage pulse with a rise time 300 ns is applied to the plates. The Rydberg atoms are field ionized by this pulse, and the ions are extracted through small holes in the upper field plate, where they are detected by a particle multiplier. The output from the multiplier is fed to two gated integrators which provide temporal resolution of the field ionization signal.

To record an anticrossing signal, the dc field is swept while all other parameters remain fixed. The integrator gates are centered on two different features of the time-resolved field ionization signal. One feature changes with the dc field and represents the signal, while the other feature remains constant and is used to normalize the signal with respect to laser power fluctuations. The red laser is run with enough power to saturate the $4s$ to $4p$ transition in order to reduce the noise.

The blackbody excited atoms are easy to distinguish from those which are excited only by the laser. First, because the blackbody excited atoms lie in higher states than the directly excited atoms, they ionize at a lower field and hence at an earlier time. Second, since the blackbody radiation is present at all times, a signal induced by it increases as T (the field ionization pulse delay) increases; the signal from the directly excited atoms decreases at T increases. The blackbody signal eventually decreases for large delays and the approximately 3 μs delay used was the value which gave the maximum signal. There was no observed dependence of the line shape on T.

A more difficult problem was the selection of the features of the time-resolved field ionization signal on which to set the gates of the integrators. The field ionization spectrum of potassium is fairly rich because the wide variety of avoided crossings encountered by each state on its path to field ionization results in a combination of diabatic and adiabatic traverses which increases the complexity of the field ionization signal.[13] In addition there are generally several states excited by the blackbody radiation. Nevertheless, it is possible by visually observing an oscilloscope signal while scanning the dc voltage through the avoided crossing to pick out features of the field ionization signal which change significantly in amplitude. This becomes more difficult for the extremely narrow crossings and it is sometimes necessary to calculate their positions by scaling from previously measured values for similar but wider crossings of lower principle quantum number n.

IV. EXPERIMENTAL RESULTS

A. s-state anticrossings

In our initial report on anticrossing signals produced by blackbody radiation[9] we presented data for the avoided crossings of the s state with the lowest-energy linear Stark manifold state for several values of the principal quantum number n. Our new data have improved resolution and cover a wider range of n. We have also measured the avoided crossings of the s state with the second-lowest Stark manifold state for a subrange of these n values. The linear manifold level with lowest energy has $l=3$ in zero electric field, and we will therefore label this level with the parabolic quantum number[14] $n_1=3$. The manifold level with second-lowest energy has $n_1=4$, and so on.

A scan of the avoided crossing of the $20s$ state with the $n=18$, $n_1=3$ manifold state is shown in Fig. 3. The horizontal scale is obtained by converting the directly measured voltages to fields, using our 1.590(1)-cm plate separation. The presence of two peaks with unequal widths is explained in Fig. 4, where we show the energy levels involved in an avoided crossing of this type. We can see from this diagram that the left-hand peak in Fig. 3 corresponds to the $|m_l|=0$ component of the $n_1=3$ manifold state, and the right-hand peak the $|m_l|=1$ component. The quantum numbers $|m_l|$ are only approximate. When we include the fine-structure interaction only $|m_j|$ is a good magnetic quantum number, and the states which we have labeled $|m_l|$ contain small admixtures of other $|m_l|$ states. If the fine-structure interaction is not included the s state crosses the $|m_l|=1$ manifold state. Therefore the right-hand peak in Fig. 3 is

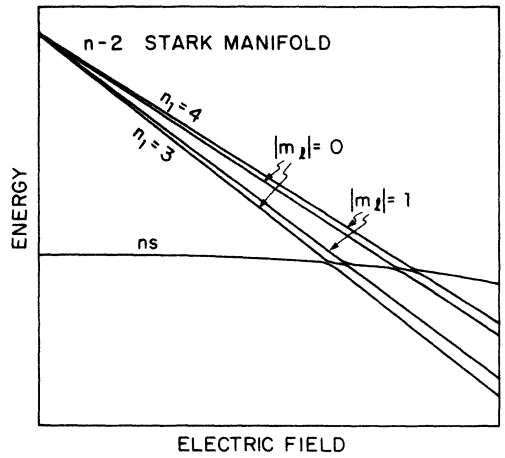

FIG. 4. Stark map for the avoided crossings of the ns state with the $n_1=3$ and $n_1=4$ states of the $n-2$ Stark manifold. The levels with higher n_1 are omitted for clarity. For each value of n_1 the nearly degenerate $|m_l|=0$ and $|m_l|=1$ levels are shown. For all levels shown $|m_j|=\frac{1}{2}$.

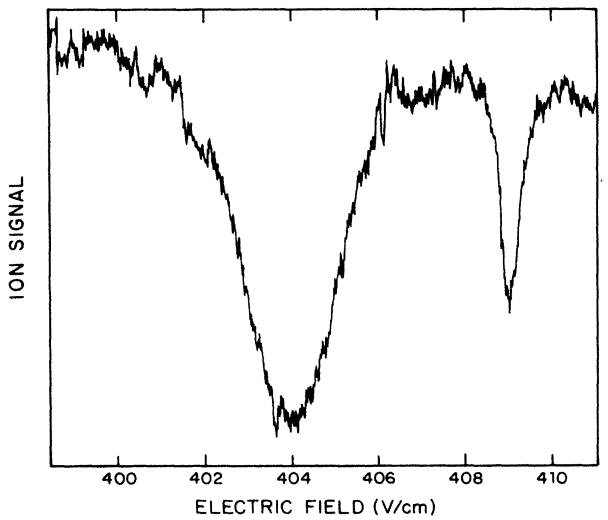

FIG. 3. Anticrossing signal from the avoided crossing of the $20s$ state with the $n=18$, $n_1=3$ Stark manifold state. The left-hand peak corresponds to the $|m_l|=0$ anticrossing, and the right-hand peak to the $|m_l|=1$ anticrossing.

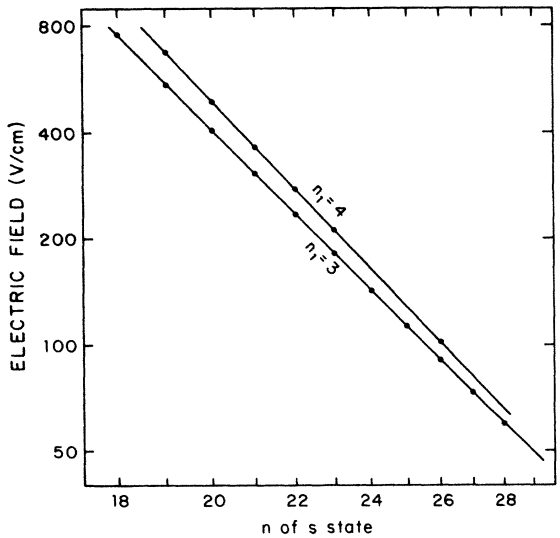

FIG. 5. Log-log plot of the observed s-state anticrossing field versus the effective quantum number n^*. Although the horizontal axis is labeled with the quantum number n of the s state, the scale is logarithmic in $n^*=n-\delta_s$. The lines are least-squares fits to the data.

TABLE I. Observed s-state anticrossing fields.

s state	$n_1=3$ $\lvert m_l\rvert=0$ (V/cm)	$n_1=3$ $\lvert m_l\rvert=1$ (V/cm)	$n_1=4$ $\lvert m_l\rvert=0$ (V/cm)	$n_1=4$ $\lvert m_l\rvert=1$ (V/cm)
18s	752.7(8)	763.5(7)		
19s	545.7(8)	553.1(5)	674.0(4)	684.0(5)
20s	403.9(5)	409.1(3)	491.1(13)	496.1(4)
21s	304.2(3)	307.9(2)	364.0(7)	367.6(3)
22s	232.7(2)	235.5(2)	275.0(4)	277.4(2)
23s	180.4(3)	182.6(2)	210.8(3)	212.6(2)
24s	141.8(2)	143.3(2)		
25s	112.5(1)	113.8(1)		
26s	90.25(8)	91.26(9)	102.7(1)	103.5(2)
27s	73.14(8)	73.90(8)		
28s	59.81(6)	60.44(5)		
29s	49.30(10)	49.78(7)		

due solely to the spin-orbit interaction. This accounts for its narrowness relative to the left-hand peak, which arises from the interaction between the Rydberg electron and the core.

The observed s-state avoided-crossing fields are given in Table I. In Fig. 5 we show a log-log plot of the s-state anticrossing field versus the effective quantum number n^* of the s state. Here $n^*=n-\delta_s$, where $\delta_s=2.18$ is the s state quantum defect. The points are the data and the lines are linear least-squares fits to the (log-log) data. Only the $\lvert m_l\rvert=0$ data are shown in the figure. The least-squares fits give the following results:

$$F=A(n^*)^P,$$

where

n_1	$\lvert m_l\rvert$	P
3	0	$-5.20(1)$
3	1	$-5.21(1)$
4	0	$-5.45(2)$
4	1	$-5.48(2)$

The exponents derived from the fits become more negative as we proceed into the manifold (i.e., as n_1 increases). We expect these exponents to be near -5 based on simple arguments. The Stark shifts [(energy)/(field)] of the manifold levels scale as $(n^*)^2$, and the zero-field energy spacing between the s state and the manifold states scales as $(n^*)^{-3}$. Therefore, if the relatively small Stark shift of the s state is ignored, the avoided crossing field is expected to scale as $(n^*)^{-5}$.

The observed widths of the s-state avoided crossings are given in Table II. In our previous report[9] the $\lvert m_l\rvert=1$ anticrossings were broadened by field inhomogeneity. The field plates used to obtain the present results have an estimated homogeneity of $\Delta F=1.0\times10^{-4}F$. A comparison with Table I shows that the widths given in Table II are not broadened by field inhomogeneity. The homogeneity was improved by using copper field plates[15] with larger area and smaller holes for ion extraction.

In Table III we compare our observed widths with theoretical widths obtained by diagonalization of the energy matrix.[8] The frequency widths are calculated directly, and are converted to field widths by using the conversion factors 356, 403, 450, and 506 MHz/(V/cm), for the 18–21s states, respectively. In all cases the observed widths are larger than the calculated widths. At least part

TABLE II. Observed widths for s-state anticrossings.

s state	$n_1=3$ $\lvert m_l\rvert=0$ (V/cm)	$n_1=3$ $\lvert m_l\rvert=1$ (V/cm)	$n_1=4$ $\lvert m_l\rvert=0$ (V/cm)	$n_1=4$ $\lvert m_l\rvert=1$ (V/cm)
18s	6.9(13)	0.63(6)		
19s	4.2(7)	0.50(6)	5.2(16)	1.0(4)
20s	2.3(2)	0.37(11)	7.5(19)	0.63(13)
21s	1.4(4)	0.23(6)	3.0(6)	0.39(9)
22s	0.9(2)	0.19(6)	1.9(3)	0.33(9)
23s	0.7(1)	0.13(6)	1.4(2)	0.28(6)
24s	0.7(2)	0.09(6)		
25s	0.6(3)	0.09(6)		
26s	0.27(6)	0.09(6)	0.38(6)	0.13(6)
27s	0.24(6)	0.09(6)		
28s	0.21(3)	0.06(3)		
29s	0.17(6)	0.08(4)		

TABLE III. Comparison of calculated and observed widths for s-state anticrossings ($n_1=3$).

	$\|m_l\|=0$			$\|m_l\|=1$		
s state	Calculated (MHz)	Calculated (V/cm)	Observed (V/cm)	Calculated (MHz)	Calculated (V/cm)	Observed (V/cm)
18s	930	5.2	6.9	80	0.45	0.63
19s	640	3.2	4.2	61	0.30	0.50
20s	450	2.0	2.3	47	0.21	0.37
21s	320	1.3	1.4	39	0.15	0.23

of this discrepancy appears to be due to the dispersion term in Eq. (12). For the $|m_l|=0$ anticrossings, the observed widths are 33, 31, 15, and 8% higher than the calculated widths for $n=18$–21, respectively. In fact our data do show progressively more asymmetric peaks for $|m_l|=0$ as we go from $n=21$ down to $n=18$.

B. p-state anticrossings

The p state also crosses the linear Stark manifold levels in potassium. In Fig. 6 we show a scan of one of these anticrossings, involving the 20p state and the $n=18$, $n_2=1$ manifold state (the manifold states are labeled, in order of decreasing energy, with the parabolic quantum number[14] $n_2=0,1,2,\ldots$). Figure 7 shows the energy levels involved in an avoided crossing of this type. Only $|m_j|=\frac{3}{2}$ levels are shown, and only the highest-energy manifold level ($n_2=0$) is shown (for both $|m_l|=1$ and $|m_l|=2$). The fine-structure interaction mixes a small amount of $|m_l|=1$ into the nominal $|m_l|=2$ manifold state. Therefore we have a situation similar to that of the s-state anticrossings. The anticrossing between the p state ($|m_l|=0$ and 1) and the $|m_l|=2$ manifold state (the peak at the right in Fig. 6) is due solely to fine structure and is consequently narrow, while the anticrossing involving the $|m_l|=1$ manifold state (the peak at the left in Fig. 6) is due to the core interaction and is much broader.

We have chosen laser polarizations which allow us to selectively populate the $|m_j|=\frac{3}{2}$ levels. The red laser is tuned to the $4s\rightarrow 4p_{3/2}$ transition, and is linearly polarized perpendicular to the electric field. This creates a 3:1 ratio of $|m_j|=\frac{3}{2}$ to $|m_j|=\frac{1}{2}$ population in the $4p_{3/2}$ state. The blue laser is linearly polarized parallel to the electric field, creating a preponderance of $|m_j|=\frac{3}{2}$ Rydberg states.

The observed p state $|m_j|=\frac{3}{2}$ anticrossing fields are given in Table IV. In Fig. 8 we show a log-log plot of the p-state anticrossing field versus the effective quantum number n^* of the p state. The points are the data and the lines are linear least-squares fits to the (log-log) data. The least-squares fits give the following results:

$$F=A(n^*)^P,$$

where

n_2	$\|m_l\|$	P
0	1	−5.18(1)
0	2	−5.21(1)
1	1	−5.30(1)
1	2	−5.35(1)
2	1	−5.48(1)
2	2	−5.53(1)

The exponents are again near −5, as they were for the s-state anticrossings. This is not surprising, since the scal-

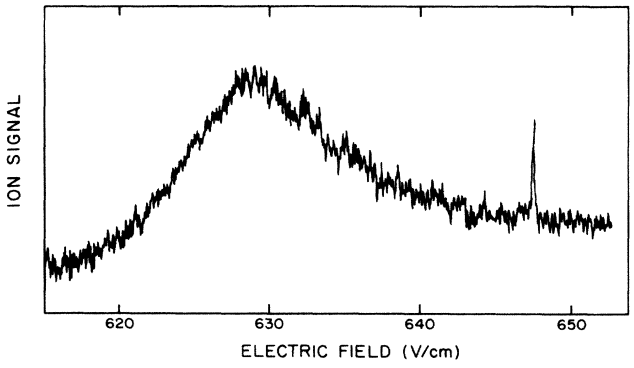

FIG. 6. Anticrossing signal from the avoided crossing of the 20p state with the $n=18$, $n_2=1$ Stark manifold state. The broad peak at the left is the $|m_l|=1$ anticrossing, and the narrow peak at the right is the $|m_l|=2$ anticrossing.

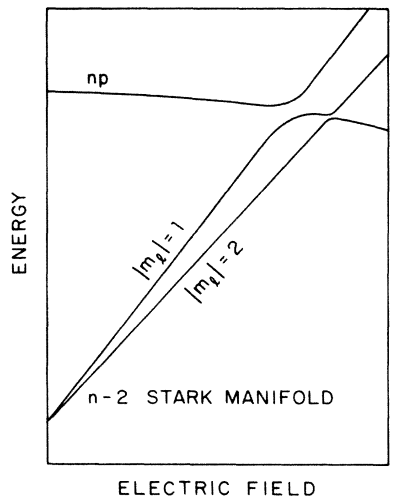

FIG. 7. Stark map for the avoided crossing of the np state with the $n_2=0$ state of the $n-2$ Stark manifold. The levels with higher n_2 are omitted for clarity. For all levels shown $|m_j|=\frac{3}{2}$.

TABLE IV. Observed p-state anticrossing fields.

p state	$n_2=0$ $\lvert m_l\rvert=1$ (V/cm)	$n_2=0$ $\lvert m_l\rvert=2$ (V/cm)	$n_2=1$ $\lvert m_l\rvert=1$ (V/cm)	$n_2=1$ $\lvert m_l\rvert=2$ (V/cm)	$n_2=2$ $\lvert m_l\rvert=1$ (V/cm)	$n_2=2$ $\lvert m_l\rvert=2$ (V/cm)
19p	737.7(13)	765.9(5)				
20p	551.8(16)	571.1(4)	627.6(8)	647.5(5)	725(3)	742.9(5)
21p	418.1(9)	432.6(3)	473.7(13)	486.7(3)	542(2)	553.4(4)
22p	321.7(7)	332.9(2)	362.0(10)	371.8(2)	410(2)	
23p	251.3(5)		280.6(7)		316(1)	

ing arguments given in the previous section for the s state apply equally well to the p states. Also, the p-state exponents become more negative as we proceed into the manifold (i.e., as n_2 increases), as did the s-state exponents.

The observed widths of the p-state $|m_j|=\frac{3}{2}$ avoided crossings are given in Table V. The $|m_l|=1$ widths vary considerably with n, while the $|m_l|=2$ widths remain relatively constant. Therefore it is safe to assume that the $|m_l|=2$ widths are limited by electric field inhomogeneity. Thus we obtain our estimate of $\Delta F=1.0\times10^{-4}F$ for the field homogeneity.

We have also observed the $|m_j|=\frac{1}{2}$ p-state anticrossings. We populate the $|m_j|=\frac{1}{2}$ Rydberg states by polarizing both lasers parallel to the electric field. In contrast to the p-state $|m_j|=\frac{3}{2}$ case, we do not observe narrow avoided crossing signals for $|m_j|=\frac{1}{2}$. This can be explained as follows. For $|m_j|=\frac{1}{2}$, there are two manifold states ($|m_l|=0$ and 1) for each value of n_2, and two p states (nominally $j=\frac{1}{2}$ and $\frac{3}{2}$). Both $|m_j|=\frac{1}{2}$ p states contain appreciable admixtures of both $|m_l|=0$ and 1. Therefore all four of the $|m_j|=\frac{1}{2}$ avoided crossings are due to core penetration and polarization. As a result these avoided crossings are relatively large. In contrast to the $|m_j|=\frac{3}{2}$ case, there are no $|m_j|=\frac{1}{2}$ avoided crossings which are due to fine structure alone. In fact the core interactions are so large that they produce a pair of "double" avoided crossings instead of four individual ones. This situation is shown in Fig. 9. As one might expect from Fig. 9, the anticrossing signals which we observe for $|m_j|=\frac{1}{2}$ are relatively complex, since each avoided crossing involves all four unperturbed levels.

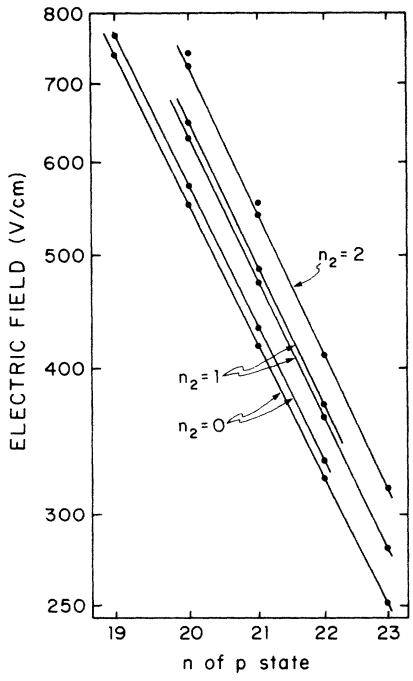

FIG. 8. Log-log plot of the observed p-state anticrossing field versus n. The lines are least-squares fits to the data.

C. Alternative experimental methods

In the course of these investigations we explored alternative schemes for the study of the avoided level crossings. The first is the obvious technique of examining the field ionization of the directly excited atoms. This signal is stronger than the blackbody signal, especially if the ionization pulse delay is reduced. The essential idea is shown in Fig. 10 for the specific case in which the excitation is primarily to the bold level. If the subsequent field ionization pulse leads to adiabatic ionization, then as the static field is swept through the crossing the ionization will

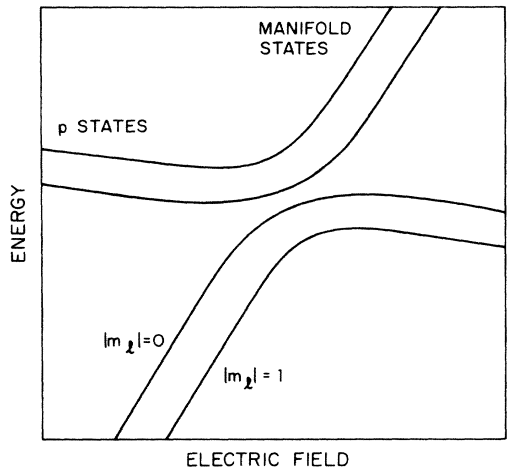

FIG. 9. Stark map for the avoided crossings of the fine structure p states with the $|m_l|=0$ and 1 manifold states, for $|m_j|=\frac{1}{2}$.

TABLE V. Observed widths for p-state anticrossings.

	$n_2=0$		$n_2=1$		$n_2=2$	
p state	$\lvert m_l \rvert =1$ (V/cm)	$\lvert m_l \rvert =2$ (V/cm)	$\lvert m_l \rvert =1$ (V/cm)	$\lvert m_l \rvert =2$ (V/cm)	$\lvert m_l \rvert =1$ (V/cm)	$\lvert m_l \rvert =2$ (V/cm)
19p	11(1)	0.06(3)				
20p	6.5(16)	0.08(5)	12(2)	0.11(3)	19(3)	0.09(3)
21p	5.2(8)	0.05(3)	8.7(13)	0.08(3)	11(2)	0.09(3)
22p	4.0(6)	0.06(3)	5.6(6)	0.05(3)	11(2)	
23p	2.6(4)		3.6(6)		8(1)	

change from occuring a point 2 to point 1. Thus if we detect ionization at point 2 (1) we would expect to observe a negative (positive) step. In practice this simple picture does not completely describe our observations. Two scans of the first s-state avoided crossing for $n=24$ are shown in Fig. 11. The laser excitation is primarily to the s state, which corresponds to the bold level in Fig. 10. The upper (lower) trace in Fig. 11 is for ionization occuring at point 2 (1) in Fig. 10. According to the above description we would expect each trace to show two steps corresponding to the $\lvert m_l \rvert =0$ and 1 avoided crossings. In fact we observe two steps with a sharp dip between them. This dip probably results from the dynamics of the field ionization pulse, preventing us from obtaining with confidence quantitative results from these direct measurements. This method does, however, provide a relatively easy way to find the approximate positions of the avoided crossings.

The second alternative method involves superradiant emission from the Rydberg state.[16] When the number of s-state Rydberg atoms is particularly high we observe an additional peak in the time-resolved field ionization signal. This peak occurs later than the normal signal, indicating that it originates from a lower-lying state. The size of the peak has a nonlinear dependence on the blue laser power. The peak disappears when we scan the dc voltage through an avoided crossing. When this noisy signal is present we also observe that the field ionization signal due to blackbody excitation to a higher state increases as we scan through an avoided crossing. Figure 12 shows an example of this effect for 20s. These observations can be explained by superradiant emission from the directly excited s state to a lower p state. This lower p state ionizes at a higher field and accounts for the extra peak in the time-resolved signal. As the dc voltage is scanned through the avoided crossing, the superradince is destroyed due to the mixing of states. The laser excitation into the s state is partially diverted into the manifold. Therefore at the avoided crossing fewer atoms are lost to

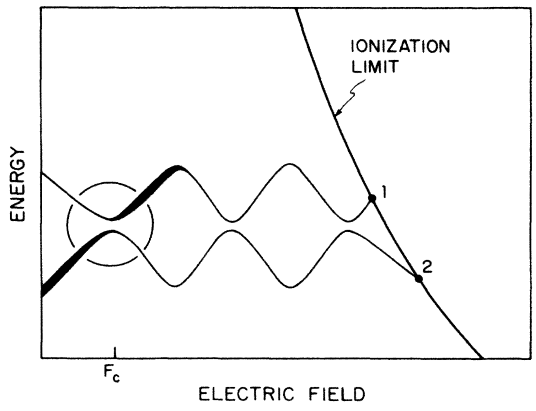

FIG. 10. Energy-level diagram for direct observation of anticrossings. The laser excitation to the circled avoided crossing is primarily to the bold level. Assuming adiabatic passage to the ionization limit, excitation with $F<F_c$ ($F>F_c$) leads to ionization at point 2 (1).

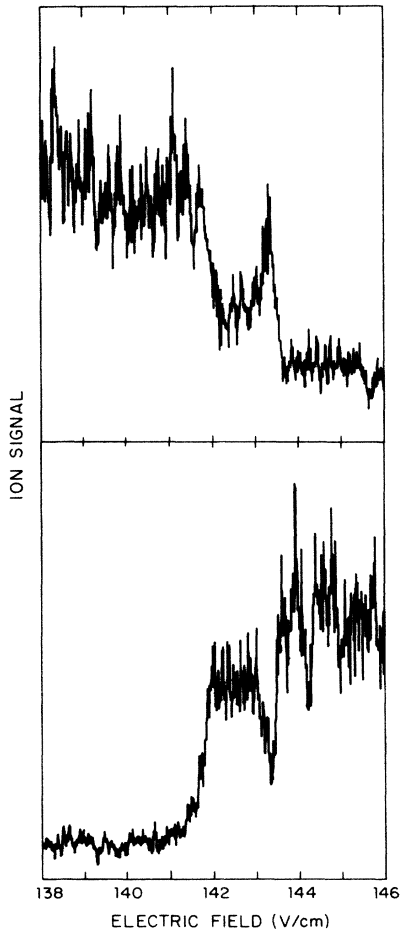

FIG. 11. Direct anticrossing signals for 24s.

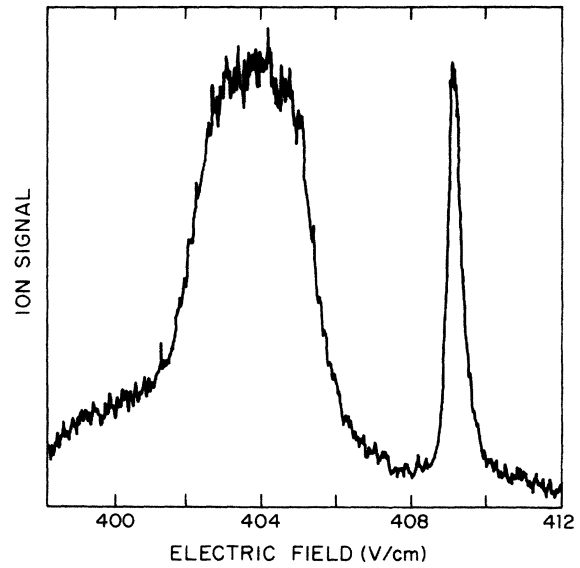

FIG. 12. Blackbody signal induced by superradiance for 20s.

superradiance, more are available for blackbody excitation, and the blackbody signal increases.

Although somewhat interesting in itself, the superradiant signal has limited quantitative usefulness due to the nonlinear nature of the superradiant emission. This saturation is evident in Fig. 12. For this reason the superradiance tended to be a nuisance. However, by keeping the number of excited atoms down we reduced this problem to a negligible level.

D. Uncertainties

There are several sources of uncertainty in these experiments. The foremost is the measurement of the plate spacing, 1.590(1) cm, which limits the absolute accuracy of the anticrossing field measurements given in Tables I and IV to roughly one part in a thousand. On the other hand, the resolution $\Delta F/F=10^{-4}$, with an absolute minimum of 0.04 V/cm, is limited by a combination of the spatial inhomogeneities, the laser spot size, and electrical pickup. This instrumental resolution has not been removed from the observed widths in Tables II and V. In most cases it is far smaller than the observed widths. We note that the field homogeneity over a larger region than the intersection of the crossed laser beams limited our day-to-day reproducibility of the anticrossing fields due to laser pointing variations. These variations however were less than uncertainty in the measurement of the plate spacing.

We extracted the anticrossing fields and widths visually from X-Y recorder tracings assuming that the anticrossing signals were symmetric Lorentzian peaks. As we have already pointed out the theoretical shape is a sum of Lorentzian and dispersion curves so this straightforward procedure is clearly not always correct, although inspection of a typical scan such as Fig. 3 suggests that it should be a reasonable approximation.

To estimate the magnitude of the error introduced by our simple analysis procedure we performed least-square fits to scans which represented both the typical nearly symmetric anticrossing signals and the most asymmetric ones. An example of the latter is the broad $|m_l|=1$ feature of Fig. 6. Fitting the data of Fig. 6 to a Lorentzian plus a dispersion curve gives a ratio of Lorentzian to dispersion of 1.6:1. The center obtained from the fit occurs at a field lower than the apparent (assuming only a Lorentzian line) center by 15% of the width, and the width obtained is less than the apparent width by 6%.

In the more typical case of Fig. 3, the errors are much less severe. Fitting the broad $|m_l|=0$ feature to a Lorentzian plus a dispersion curve shows that the ratio of their amplitudes is greater than 10:1, that the fit center differs from the apparent center by 3% of the width, and that the fit width is less than 3% smaller than the apparent width. In all cases the errors introduced by our method of analysis are less than the other uncertainties in the data. The stated uncertainties in the tables include those due to the analysis.

In principle we should be able to calculate the ratio of Lorentzian to dispersion in our signals by using Eq. (12), with the f and g values given by the method of Ref. 8. In practice, however, there is uncertainty in identifying the final states excited by the blackbody radiation, due to the complexity of the field ionization of potassium. For example, the final state for the s-state anticrossings is in principle a p state, but several nearby manifold levels contain appreciable admixtures of p character. Since the field ionization is not selective enough to distinguish between the p state and the nearby levels we cannot calculate the g values.

V. CONCLUSION

We have demonstrated a new method of anticrossing spectroscopy using pulsed excitation and a combination of blackbody radiation and field ionization for detection. We have used this method to measure avoided crossings between Stark levels of highly-excited potassium atoms. This method is complementary to the purely laser spectroscopic method and is particularly useful where the width of the avoided crossing is less than the laser width.

ACKNOWLEDGMENT

This work was supported by the Air Force Office of Scientific Research under Grant No. AFOSR-85-0016.

[1]F. D. Colegrove, P. A. Franken, R. R. Lewis, and R. H. Sands, Phys. Rev. Lett. 3, 420 (1959).

[2]T. G. Eck, L. L. Foldy, and H. Weider, Phys. Rev. Lett. 10, 239 (1963).

[3]K. C. Brog, T. G. Eck, and H. Wieder, Phys. Rev. 153, 91 (1967).

[4]W. Nagourney, W. Happer, and A. Lurio, Phys. Rev. A 17, 1394 (1978).

[5]P. Hannaford and G. W. Series, Phys. Rev. Lett. **48**, 1326 (1982).
[6]J. R. Rubbmark, M. M. Kash, M. G. Littman, and D. Kleppner, Phys. Rev. A **23**, 3107 (1981).
[7]H. B. Van Linden Van den Heuvell, R. Kachru, N. H. Tran, and T. F. Gallagher, Phys. Rev. Lett. **53**, 1901 (1984).
[8]M. L. Zimmerman, M. G. Littman, M. M. Kash, and D. Kleppner, Phys. Rev. A **20**, 2251 (1979).
[9]R. C. Stoneman, T. F. Gallagher, Phys. Rev. Lett. **55**, 2567 (1985).
[10]W. E. Cooke and T. F. Gallagher, Phys. Rev. A **21**, 588 (1980).
[11]S. Haroche, M. Gross, and M. P. Silverman, Phys. Rev. Lett. **33**, 1063 (1974).
[12]T. F. Gallagher, L. M. Humphrey, W. E. Cooke, R. M. Hill, and S. A. Edelstein, Phys. Rev. A **16**, 1098 (1977).
[13]T. F. Gallagher and W. E. Cooke, Phys. Rev. A **19**, 694 (1979).
[14]L. D. Landau and E. M. Lifshitz, *Quantum Mechanics: Non-relativistic Theory,* 3rd ed. (Pergamon, New York, 1977), p. 130.
[15]T. W. Ducas, W. P. Spencer, A. G. Vaidyanathan, W. H. Hamilton, and D. Kleppner, Appl. Phys. Lett. **35**, 382 (1979).
[16]M. Gross, P. Goy, C. Fabre, S. Haroche, and J. M. Raimond, Phys. Rev. Lett. **43**, 343 (1979).